Research Article | Vol. 27, No. 5 | 4 Mar 2019 | OPTICS EXPRESS 6068
Optics EXPRESS

Breaking diffraction limit of far-field imaging via structured illumination Bessel beam microscope (SIBM)

SANDEEP MENON PERINCHERY,[1,2] ASWIN HARIDAS,[1,2] ANANT SHINDE,[2] OLEKSANDR BUCHNEV,[3] AND VADAKKE MATHAM MURUKESHAN[1,2,*]

[1]*School of Mechanical and Aerospace Engineering, Nanyang Technological University, Singapore, 639798, Singapore*
[2]*Centre for Optical and Laser Engineering, 50 Nanyang Avenue, Singapore 639798, Singapore*
[3]*Optoelectronics Research Centre, University of Southampton, Building 53 University Road, Highfield Southampton S017 1BJ, UK*
[*]*mmurukeshan@ntu.edu.sg*

Abstract: Breaking the diffraction limit in imaging microscopes with far-field imaging options has always been the thrust challenge for optical engineers and biologists over the years. Although structured illumination microscopy and Bessel beam assisted imaging has shown the capability of imaging with sub-diffraction resolutions, they rely on the use of objective lenses with large numerical apertures (NA). Hence, they fail to sustain resolutions at larger working distances. In this context, we demonstrate a method for nanoscale resolution imaging at longer working distances, named as Structured Illumination Bessel Microscopy (SIBM). The proposed method is envisaged for both biological and engineering applications that necessitate high imaging resolutions at large working distances.

1. Introduction

There are a number of far-field optical imaging techniques that are capable of achieving sub-diffraction resolution [1–3]. Far-field sub-diffraction resolution microscopy techniques such as structured illumination microscopy (SIM) [4,5], stimulated emission depletion microscopy (STED) [3–6], stochastic optical reconstruction microscopy (STORM) [7], photo activated localization microscopy (PALM) [8], field independent imaging (FIFI) [9] and reversible saturable optical linear fluorescence transitions (RESOLFT) [10] have revolutionized cellular imaging. Many new imaging devices have been reported or introduced recently for sub-wavelength resolution imaging which includes metamaterial superlens [11–13] and hyperlens [14]. Despite all these advancements, there is still an important constraint to overcome in many high resolution microscopy applications. This is mainly attributed to the fact that these reported techniques fail to attain the same resolution at larger working distances. Most of these microscopy methods which generally attain sub-diffraction resolution rely on objective lenses with a large numerical aperture (NA), such as 100 X, NA = 1.2. However, they have very small working distances which are in the order of 0.1 mm to 0.3 mm between the lens plane and the object plane, limiting its applicability. In classical wide field microscopy, this is a fundamental problem while designing any high resolution systems.

The recently developed Bessel beam microscope (BBM) system by Snoeyink *et al*, has used unstructured broadband illumination to attain sub-diffraction limited imaging by incorporating a convex lens in series with an axicon lens in the optical path of a microscope [15,16]. The non-diffractive nature of the Bessel beam plays a major role in the BBM system [17]. BBM is indeed a simple approach proposed to improve the resolution of a conventional wide field microscope by at least one third. This is achieved by narrowing the peak of the point spread function (PSF). Here, we demonstrate the experimental implementation of a BBM modified with a structured illumination unit. An illustrative imaging analysis

#352479 https://doi.org/10.1364/OE.27.006068
Journal © 2019 Received 22 Nov 2018; revised 7 Jan 2019; accepted 8 Jan 2019; published 20 Feb 2019

Optics EXPRESS

confirming far field sub-diffraction resolution at large working distances was tested in both reflection and fluorescence configurations by the newly developed SIBM system. A comparison of the spatial features resolvable by a longer working distance objective (50 X; 0.55 NA) using BBM and our proposed SIBM method is provided. The results confirm that at larger working distance, the resolution achievable with SIBM is superior compared to conventional wide field microscope and BBM configuration.

2. Materials and methods

2.1 Optical design of structured illumination Bessel microscope system (SIBM)

Figure 1 shows the schematic diagram of the SIBM. A multiline laser source combiner with diode lasers of wavelengths 488 nm, 514 nm and 561 nm serve as excitation sources (Coherent Inc, OBIS laser, USA). A 50X Nikon TU Plan ELWD corrected long working distance microscope objective (50X, NA 0.55, 11 mm working distance) was used as the objective lens. Light modulated by a transmissive liquid crystal spatial light modulator (SLM; HOLOEYE, LC 2012) after passing through a polarizer was reflected by a dichroic beam splitter onto the back aperture of the microscope objective. The light from the microscope objective lens was then collected through a tube lens (ITL 200, Thorlabs). A convex lens (LB-1844-A, Thorlabs, F = 50 mm) was placed at the focal plane of the tube lens. An axicon lens with $\alpha = 2°$ was placed approximately 1 cm from the convex lens. The combination of convex lens and axicon lens is known to transform the wave front of a point source into a Bessel beam, which has a unique property to propagate without diffraction. In the fluorescence configuration, the reflected laser beam is separated from the fluorescence beam passing through the axicon lens by a filter and finally captured by the EMCCD camera (iXON 887 Andor, Canada). An additional biconvex lens (LB-1901, Thorlabs, F = 75 mm) was also placed 85 mm away from the axicon. Conceptual ray trace of the BBM configuration using Zemax© is shown in Appendix A (Fig. 7).

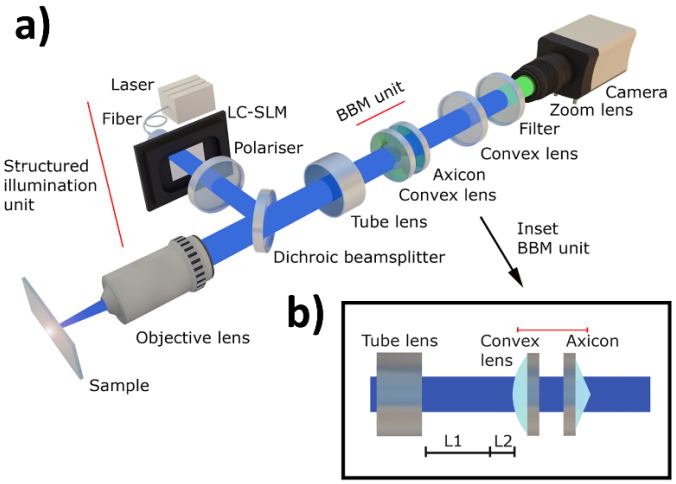

Fig. 1. (a) Shows the schematic of the SIBM microscope configuration and the inset (b) illustrates the BBM unit. Here, L1: focal length of tube lens (ITL 200, Thorlabs, F = 200 mm); L2: focal length of convex lens (LB-1844-A, Thorlabs, F = 50 mm). LC-SLM is liquid crystal spatial light modulator (HOLOEYE, LC 2012).

For measurements performed using the conventional BBM arrangement, unstructured broadband illumination was utilized, i.e., no light pattern was generated by the SLM (switch off -mode). In contrast, while performing measurements in the SIBM configuration, the

Optics EXPRESS

illumination patterns were projected using SLM (switch on-mode). Using a LabVIEW program, the camera, SLM and microscopic stage were automated to sequentially project different grating patterns and perform image acquisition.

2.2 Structured illumination and image processing

For SIBM configuration, we used a transmissive SLM (HOLOEYE LC2012) to generate the illumination patterns. The SLM is based on a Liquid Crystal (LC) micro-display with 1024 X 768 pixels. This LC-SLM can change the grayscale level of any pixel between 0 and 255 with a switching rate of 60 Hz. Three images were captured using an EMCCD camera with the phase of the illumination pattern shifted 120° between them. This method was repeated for two more orientations of the illumination pattern rotated by 120° and 240°. Figure 2 shows the nine patterns loaded onto the LC-SLM to generate the respective illumination pattern. The variation in the grayscale levels of the sinusoidal patterns is shown in Fig. 2(b).

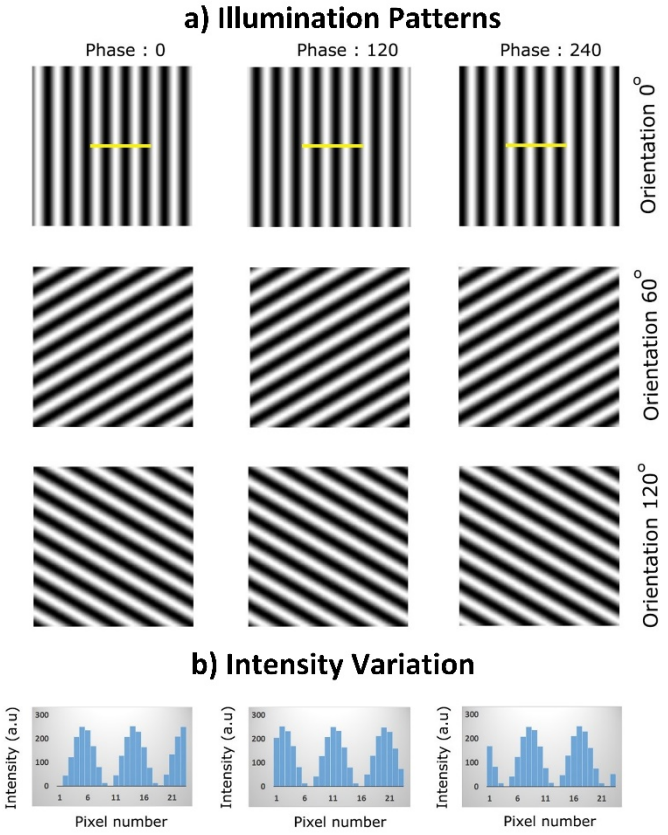

Fig. 2. (a) shows the patterns projected onto the LC-2012, SLM to modulate the illumination and (b) Illustrates the variation of the grayscale levels in the LC-SLM pixels along the illumination patterns for orientation 0° with phase shifts of 0°, 120° and 240°, respectively, marked using a yellow line in (a).

The resultant image is calculated using the relation [18],

$$I_p = \left[(I_1 - I_2)^2 + (I_2 - I_3)^2 + (I_1 - I_3)^2 \right]^{1/2} \quad (1)$$

Here, I_1, I_2 and I_3 are the three images captured using the illumination patterns phase shifted at 0°, 120° and 240°, respectively. I_p is the resultant image determined from the three

Optics EXPRESS

phase shifted images. Finally, to subdue the noise in the images, deconvolution was performed using an Iterative Parallel Deconvolution plugin using the ImageJ software.

2.3 Sample preparations

For the resolution measurements, the test sample used was TetraspeckTM fluorescent microspheres of diameter 0.2 µm (λ_{Ex} = 561 nm and λ_{Em} = 580 nm) on a 170 µm thick coverslip. We have used the fixed muntjac skin fibroblast and BPAE cells (Thermo Fisher Scientific) as the biological test samples. The BPAE cells was labelled with the fluorescent dye, Alexa Fluor 488 wheat germ agglutinin (λ_{Ex} Peak = 490 nm, λ_{Em} Peak = 525 nm). Mitochondria of the muntjac cells were labelled with an anti–OxPhos Complex V inhibitor protein mouse monoclonal antibody in conjunction with Alexa Fluor 555 goat anti–mouse IgG (λ_{Ex} Peak = 561 nm, λ_{Em} Peak = 570 nm). The reference SEM image of the Siemen's star test chart used in our study is illustrated in Appendix C (Fig. 10). The Siemen's star test chart was etched using the Focused Ion Beam (FIB) technique.

3. Results and discussions

3.1 Spatial resolution of SIBM system in fluorescence configuration

The SIBM fluorescence microscope is illustrated in Fig. 1. Briefly, a 561 nm Gaussian laser beam modulated by the transmissive SLM projects grating patterns onto the sample through a microscope objective lens. The camera collects the fluorescence signals from the sample through the BBM unit, which include the convex lens and the axicon. Further, processing techniques are implemented for image reconstruction.

In order to evaluate the spatial resolution of the SIBM setup, we first imaged TetraspeckTM fluorescent microspheres (0.2 µm, λ_{Ex} = 561 nm and λ_{Em} = 580 nm) on 170 µm thick coverslips. For wavelengths 561 nm and 580 nm, the Rayleigh's resolution limit for the 50X microscope objective with NA 0.55 and a 11 mm working distance is calculated using Eq. (2) as, 622.2 nm and 643.3 nm, respectively [1]. Since the sizes of the beads are lower than the resolution limit of the objective lens used, the capability of the system to resolve individual particles can prove sub-diffraction resolutions can be achieved [1,4].

$$\text{Rayleigh Resolution} = \frac{0.61 \times \lambda}{NA} \tag{2}$$

Here, λ is the wavelength of light while NA is the Numerical Aperture of the objective lens used. Figure 3(a) shows the 200 nm bead images obtained using the BBM configuration while, Fig. 3(b) and 3(c) shows the deconvolved 200 nm bead images obtained by BBM and the SIBM microscope configurations, respectively. A comparison of the measured lateral resolutions for the two configurations is shown in Fig. 3(d). The measurement is done by averaging the data obtained from 20 fluorescent nanobeads. As evident from Fig. 3(d), the lateral resolution obtained for SIBM is 378 ± 20 nm, which is far superior to that obtained with a BBM configuration (450 ± 15 nm). Figure 3(e) also presents a better separation between 200 nm beads imaged with the SIBM system, illustrated using a line profile. These results clearly show an improvement in lateral resolution for the conventional BBM configuration when combined with structured illumination.

Optics EXPRESS

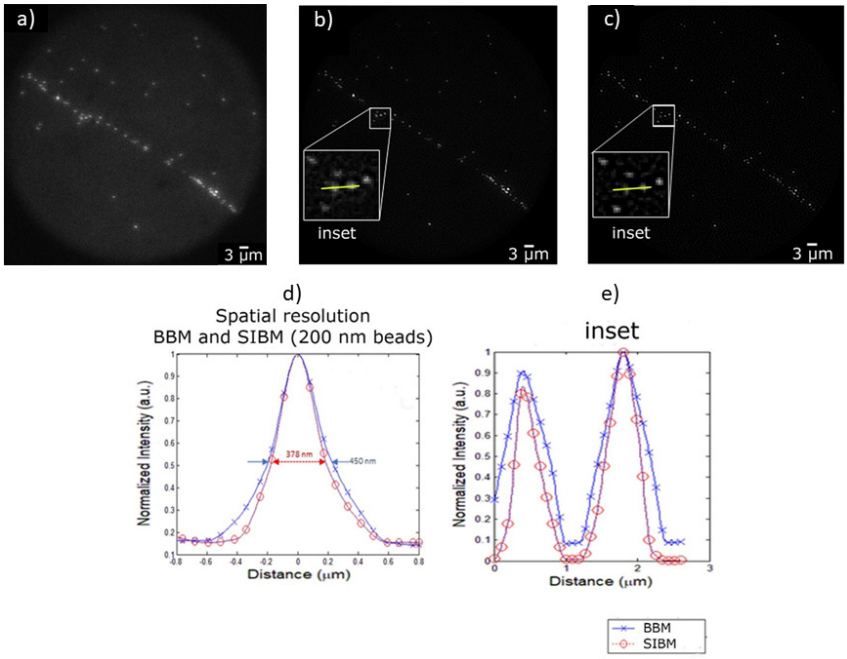

Fig. 3. The lateral resolution measurements were performed using 0.2 μm Tetraspeck fluorescent microspheres (λex = 561 nm and λem = 580 nm) on 170 μm thick coverslips. A561 nm laser was used for exciting the microspheres. (a) shows the raw image captured using the BBM configuration. As a comparison, (b) shows the 0.2 μm Tetraspeck. Fluorescent microspheres are captured and deconvolved using the BBM microscope, while (c) shows the deconvolved image captured by using the SIBM microscope. An average PSF taken from 20 microspheres from both the BBM and SIBM configuration is plotted in (d). The profile along the yellow lines indicated in the insets within (b) and (c) is plotted in (e).

Biological cell was imaged using the SIBM fluorescence imaging configuration. Figure 4(a) shows the fluorescence image of a fixed, permeabilized, and labelled muntjac skin fibroblast (FluoCells prepared slide #6 muntjac cells, Thermo Fisher Scientific) captured using the raw BBM configuration. Further, Figs. 4(b) and 4(c) shows the deconvolved images captured with BBM and SIBM, respectively. Mitochondria in the muntjac cells were labelled with Alexa Fluor 555 goat anti–mouse IgG which having 561 nm excitation and 571 nm emission wavelengths. As compared to BBM, the fluorescence image of muntjac mitochondria captured using SIBM system has a better spatial resolution. This improvement in resolution can also be observed in the line profiles illustrated with dotted lines, shown in Fig. 4(d).

Optics EXPRESS

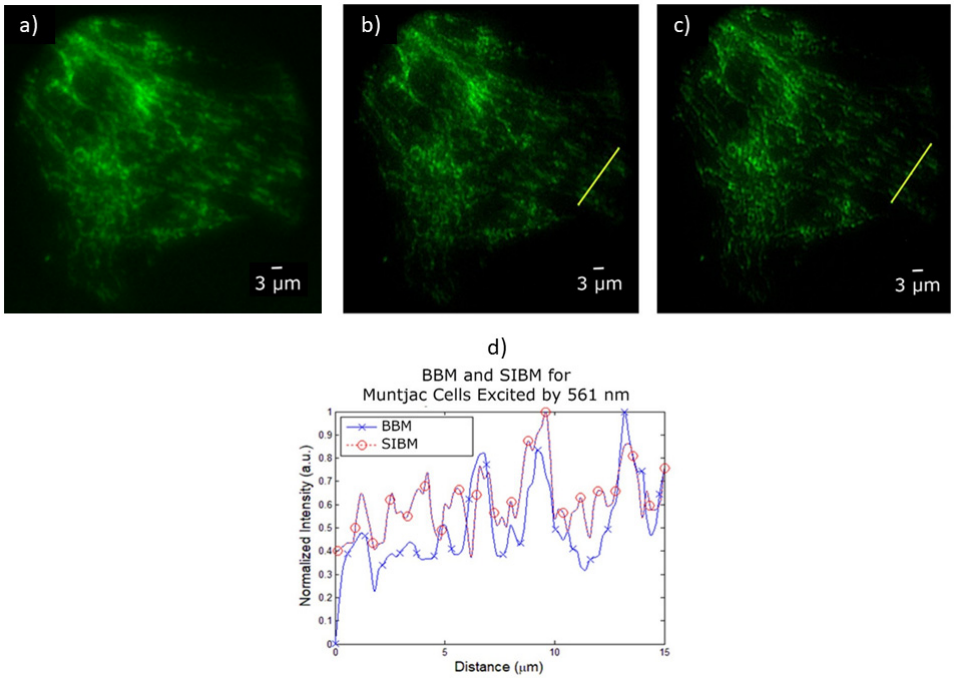

Fig. 4. (a) shows the raw image of the Muntjac cells captured using the BBM configuration. As a comparison, (b) shows the deconvolved image captured using the BBM configuration and (c) shows the Image captured using the SIBM configuration. The yellow line indicated over (b) and (c) at the same location is plotted as intensity Vs. position in (d).

Further, the improvement in lateral resolution of the SIBM system as compared to a conventional widefield microscope configuration is validated by imaging bovine pulmonary artery endothelial cell (BPAE cells) slices, shown in Fig. 5. The BPAE cells have been labelled with MitoTracker Red CMXRos for mitochondria. They are then fixed, permeabilized and stained with Alexa Fluor 488 phalloidin for F-actin. It can be observed that the respective fluorescence images of mitochondria and F-actin were clearly visible with 561 nm and 488 nm excitations. Figure 5(c) clearly shows the improved lateral resolution of SIBM over conventional wide-field microscopy.

From these results, it is evident that the lateral resolution of SIBM configuration is better than BBM and basic widefield microscope configuration. Moreover, it can be inferred that the overall fluorescence lateral resolution of the system can be further improved by using a larger NA microscope objective, compromising the larger working distance in this proposed SIBM configuration.

Optics EXPRESS

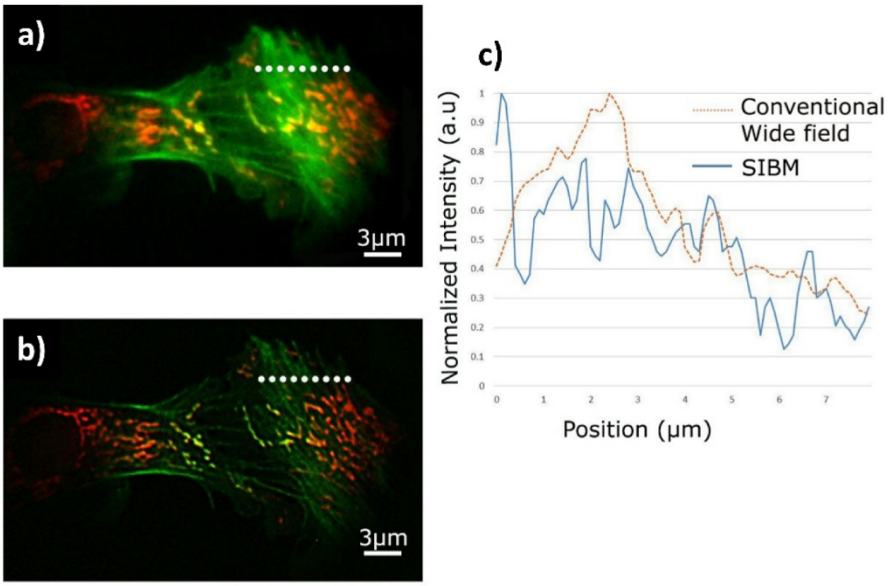

Fig. 5. (a) shows the image of BPAE cells captured using the conventional wide field microscope and (b) shows the image captured using the SIBM configuration. The dotted line scans indicated in white color over the images at the same location in (a), (b) is plotted as intensity Vs. position in (c).

3.2 Spatial resolution of SIBM system in reflection configuration

In order to numerically quantify the spatial resolution of the SIBM system in the reflection configuration, we captured images of a Siemen's star. The spokes of a Siemen's star approximate a radially varying assessment of spatial frequencies considering the system aberrations. As in the fluorescence configuration, a 561 nm illumination wavelength was used for measurements. The results of the Siemen's star image patterns are shown in Fig. 6. It is evident from Fig. 6(a) that the microscope with structured illumination in the reflection mode (without the BBM unit) has a resolution of around 595 ± 5 nm. In contrast, SIBM has improved the lateral resolution to about 505 ± 5 nm, shown in Fig. 6(b). It is clearly evident from these results that the SIBM in the reflection mode imaging provide sub-diffraction resolution.

Notably, Siemen's star images captured by a standard laser scanning confocal microscope (Zeiss, LSM 800) with a microscope objective 60X 1.4 NA air (Nikon, high NA, short working distance of 0.13 mm) at 561 nm also have comparable results to the developed SIBM system having microscope objective 50X 0.55 NA air and 11 mm long working distance, see Fig. 6(c). However, it is to be noted that in comparison to the SIBM in fluorescence configuration, the reflection mode has a poor lateral resolution. This reduced resolution in the reflection mode is mainly attributed to the noise introduced by laser speckle and scattering.

Multiple implementations of structured illumination have been described in the literature that includes super resolution SIM (SR-SIM) and optical sectioning SIM (OS-SIM). Whilst the former has shown up to a two-fold improvement in lateral resolution, the latter discussed the improvement in resolution by removing the background noise [4,18]. The concept of lateral resolution improvement using SR-SIM has been well understood using the concept of the moiré effect. Here, the sample is illuminated by a set of structured illumination patterns as shown in Fig. 2(a) which results in moiré fringes in the emission distribution. Knowing the position, orientation and period of the illumination grid, the sub-diffraction fine structures on a sample can be recovered as the moiré [1,4]. In contrast, for OS-SIM implementation, the emission distribution of the sample illuminated using the same set of structured grids contain

Optics EXPRESS

both in-focus and out-of-focus information. Since the out-of-focus information is not modulated via structured illumination, the in-focus information can be estimated by removing the grid patterns [18]. Even though OS-SIM does not offer lateral resolution improvements as compared to SR-SIM, the ease of implementation and data processing makes it an important candidate for high resolution biological and engineering samples. In this study, we have used the optical sectioning algorithm for processing the images. Fourier-based super resolution SIM reconstruction was not used on the captured images. This is due to the slight swirling of the image caused by the inherent property of axicon lens in the imaging arm (see Appendix D, Fig. 13). Moreover, SIBM unit also introduces a magnification factor of 1.4 in the current setting as compared to conventional microscope, see Appendix D (Fig. 12). This would require recalibration of the frequency of grating lines to enhance the resolution in case of frequency-based SIM process. To reduce the distortion caused by swirling, we have used axicon lens with small physical cone angle.

The speed of data acquisition of the SIBM, is mainly limited by the speed and sensitivity of the CCD camera and LC- SLM switching time. The LC-SLM switching frequency is 60 Hz, thus has a negligible impact on the speed of data acquisition. However, the use of DMD (switching frequency 10,000 Hz) instead of LC-SLM is an alternate option to improve the data acquisition speed. In the current version, we used 512 x 512 pixels EMCCD camera (iXON 887 Andor) with a maximum full-frame rate of 25 fps. However, the use of high speed sCMOS cameras such as the Neo, Andor (100 fps) can improve the overall system speed.

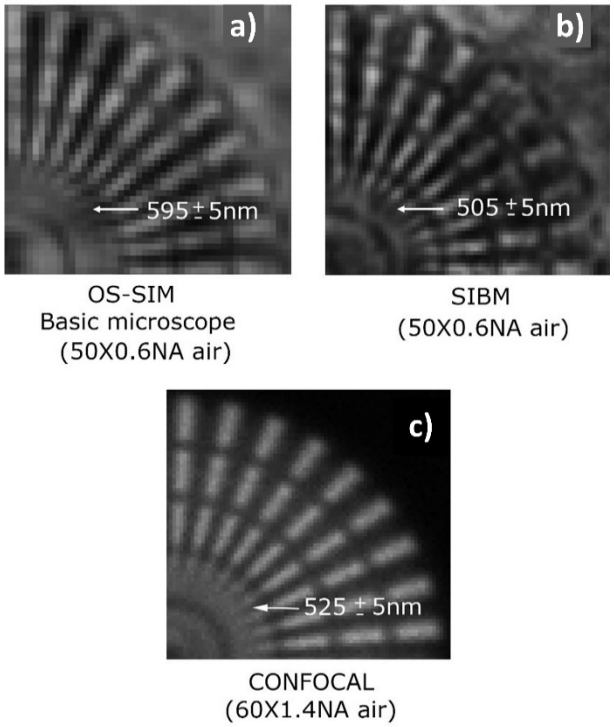

Fig. 6. Measurement of the SIBM lateral resolution using Siemen's star as the test target. (a) shows the raw image captured using the basic microscope configuration with SIM, (b) shows the raw image captured using the SIBM configuration and (c) is the raw image captured using the standard laser scanning confocal microscope. Zeiss, LSM 800 laser scanning confocal microscope with 1.4 NA 60X air objective (Nikon, high NA, short working distance of 0.13 mm) was used to capture the image. The reference Siemen's star details are provided in Appendix C (Fig. 10).

Optics EXPRESS

4. Conclusion

We have demonstrated a novel SIBM microscope system, capable of direct high quality far field fluorescence and reflection imaging with sub-diffraction resolution. It is to be emphasized that we have performed this high resolution imaging using longer working distance objective in the wide field configuration. The resolution can be improved even further by optimizing the imaging conditions such as by choosing fluorescent dyes, higher NA objective and by reducing photo-bleaching with faster data acquisition. It is envisaged that this proposed microscope concept has the potential to be used for high resolution microscopy applications in a variety of fields which require longer working distances.

Funding

MOE (RG162/15) and COLE-EDB.

Acknowledgments

We would like to acknowledge the fruitful discussions with Professor Nikolay Zheludev (University of Southampton) and his support. S.M.P. along with VMM designed and developed the research presented in this manuscript. SMP, AH and AS performed experiments, image processing and analysed the data along with VMM. Custom Siemen's star target was designed and fabricated by OB. VMM corrected and revised the manuscript contents prepared by SMP and AH. All authors prepared, read and approved the final manuscript. VMM advised and supervised the research as principal investigator of the project. The research was performed when the authors SMP and AS were research staffs attached to VMM at the Centre for Optical and Laser Engineering (COLE), Nanyang Technological University. The authors declare no competing financial interests.

Appendix A: optical ray diagram

Figure 7 shows optical ray diagram of the basic microscope configuration and its modified configuration with an additional BBM unit. In this simulation, for all the individual optical elements we have utilized the original Zemax© files provided by Thorlabs. It is to be noted that, instead of the 50X, NA 0.55 Nikon TU Plan ELWD corrected long working (11 mm) distance microscope objective used for our experimental setup, a 4X Super Apochromatic microscope objective, 0.2 NA, 17.2 mm WD the objective lens was used for the simulation. The is because the Zemax© model for the former was unavailable. An illumination of 561 nm wavelength was used for this simulation study. As shown in Fig. 7(a), the microscopic objective lens was placed at the focal plane of the point source. In the Fig. 7(b), the convex lens (LB-1844-A, Thorlabs, F=50 mm) was placed at the focal plane of the tube lens. LB-1901 biconvex lens (Thorlabs, F=75 mm) was positioned 85 mm away from the axicon lens.

Optics EXPRESS

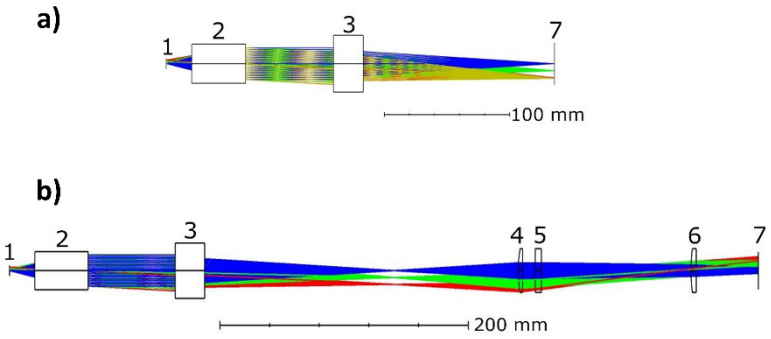

Fig. 7. Optical ray tracing using Zemax© (a) and (b) shows the ray diagram of the basic microscope configuration and ray tracing for the BBM unit with axicon lens assembly, respectively. [1: point source illumination; 2: microscopic objective dry lens (Thorlabs, 4X Super Apochromatic, 0.2 NA, 17.2 mm WD); 3: tube lens (Thorlabs, TTL200 - Tube Lens, f = 200 mm, ARC: 350-700 nm); 4: convex lens (LB-1844-A, Thorlabs, F = 50 mm); 5: axicon lens (Thorlabs axicon lenses AX252-A, α = 2o); 6: biconvex lens (LB-1901, Thorlabs, F = 75 mm); 7: detector).

Appendix B: point spread function (PSF)

Figure 8 shows the comparison of point spread function of a conventional microscope configuration and its modified version with the BBM unit. As earlier demonstrated by Snoeyink et al, the BBM unit improves the resolution of the conventional wide field microscope by narrowing the peak of point spread function (PSF) [15,16]. It is also evident from our optical simulation that there is a reduction in the PSF when the BBM unit is attached to the conventional microscopic configuration (Fig. 8).

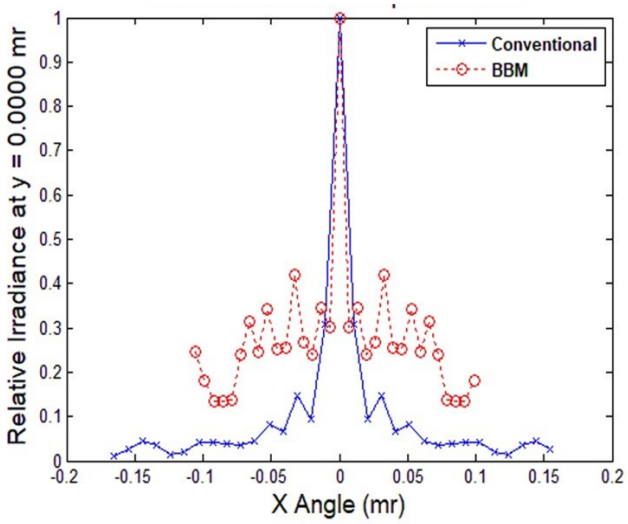

Fig. 8. Comparison of Point spread function (PSF) of a conventional microscope and a Bessel Beam Microscope

Axicon lens is known to generate Bessel like non-diffractive beams. The properties of these beams mainly depend on the physical angle of the axicon lens. In order to understand the influence of the physical angle of the axicon lens on the PSF of the imaging system, we performed multiple Zemax© simulation using different axicon lenses. As shown in Fig. 7, for the optical simulation of the microscope configuration with the BBM unit, we tested changes

Optics EXPRESS

in PSF with axicons having different physical angles. It is evident from Fig. 9 that the PSF reduces with higher physical angles of the axicon lens.

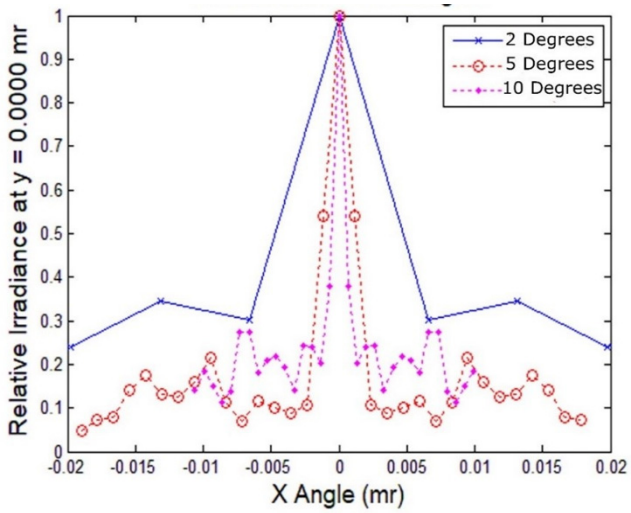

Fig. 9. Variation in PSF with different axicon angles. Represents the PSF measured with respect to the physical angle of the axicon lens used. In this simulation we have used Thorlabs axicon lenses AX252-A, AX255-A, AX2510 having axicon angles 2°, 5° and 10^0 respectively.

Appendix C: white light transmission imaging to test BBM imaging unit

For SIBM in fluorescence configuration, defining resolution is straight forward. We have used fluorescence beads to measure the PSF of the SIBM system. However, for measuring the resolution of the coherent SIBM system in reflection configuration is more complex. As recommended by Roarke Horstmeyer *et al*, use of a standard spoke-pattern imaging target is important to measure the resolution of microscope in coherent refection mode [19]. Hence, in this study we have used the Siemen's star to test the resolution of the SIBM system. Figure 10 shows the SEM image of Siemen's star utilized in our study.

Optics EXPRESS

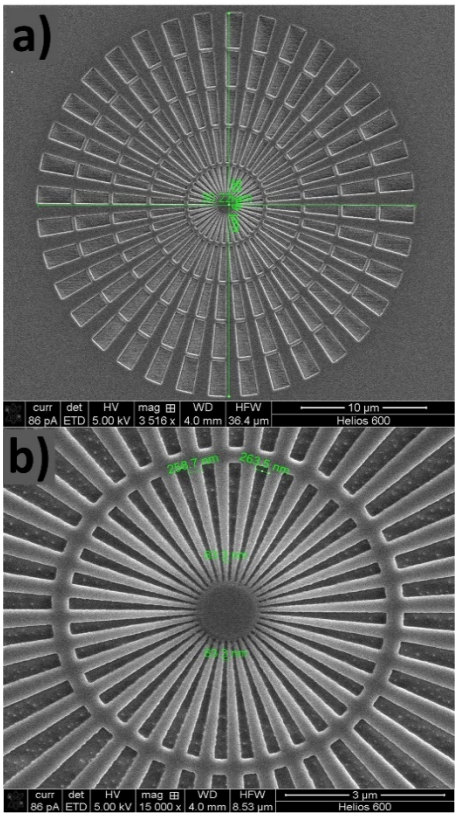

Fig. 10. Siemen's star test chart (a) Scanning electron microscopy image of Siemen's star and (b) illustrates the zoomed image of the inner spokes of Siemen's star.

In the main manuscript, we have described the reflection and fluorescence configuration of the SIBM system with the BBM unit. Figure. 11 shows the transmission image of Siemen's star imaged using the basic microscopic with and without BBM unit. Here we have used an unstructured laser beam having a 561 nm wavelength to illuminate the Siemen's star. Figure 12 shows the circular profile of the captured Siemen's star. It is evident from Fig. 11. and Fig. 12. that BBM improves the resolution of the system. In addition, there is also 1.4 times increase in magnification for the BBM configuration. It is important to note that we have not used structured light in transmission configuration.

Optics EXPRESS

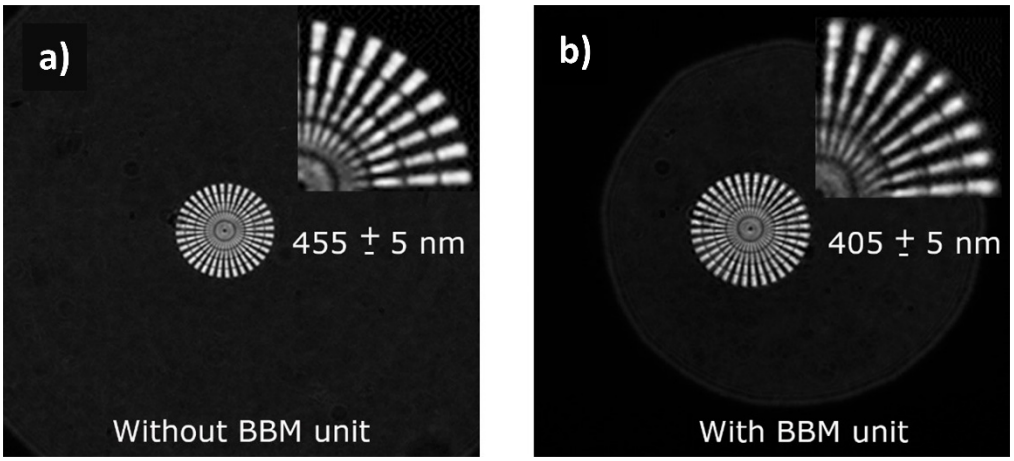

Fig. 11. (a) Siemen's star Imaged in the transmission mode using the basic microscope configuration and (b) using the basic microscope configuration modified with the BBM unit.

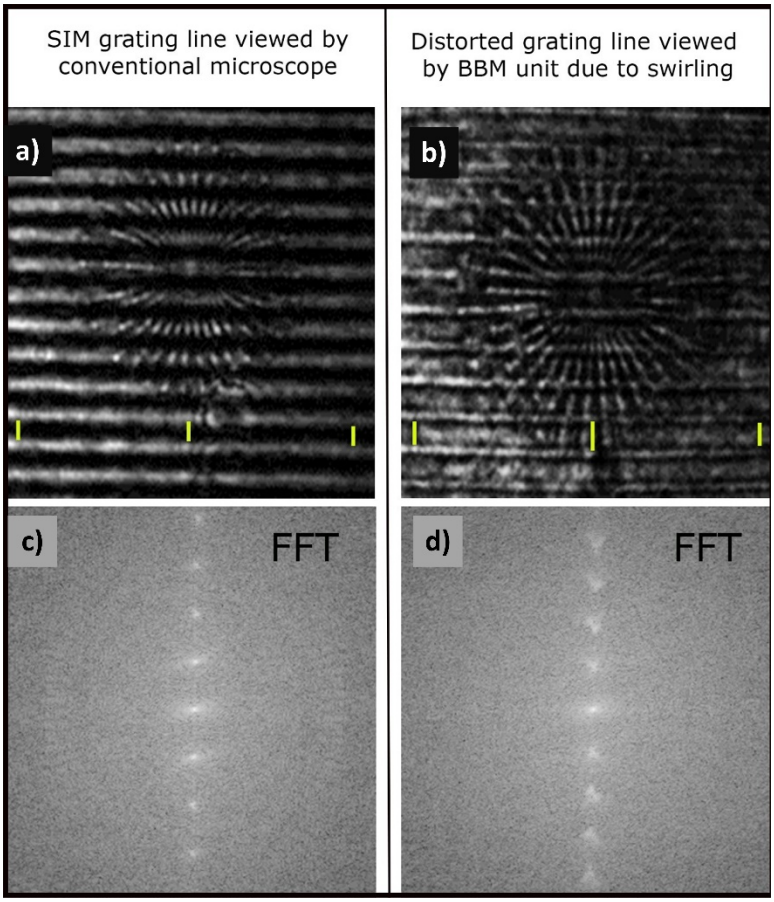

Fig. 12. (a) Siemen's star imaged using the basic microscope configuration and (b) using the basic microscope configuration modified with the BBM unit. The profile of the circular section of the Siemen's star indicated by the green circle in (a) and (b) is shown in (c) and (d).

Optics EXPRESS

Appendix D: swirling by axicon lens

As described in Appendix B, the PSF of the imaging system can be narrowed by selecting an axicon lens with a higher physical angle (α). Importantly, an image captured using an axicon lens is known to be affected by swirl (haze) [17,20]. Higher physical angles of the axicon lens will result in an increased image swirl. Typical example of the swirling problem caused by the axicon configuration is illustrated in Fig. 13. Image of the Siemen's star illuminated by grating lines taken by basic microscope configuration is presented in Fig. 13(a). The same image visualized by the microscope modified with SIBM unit is shown in Fig. 13(b).

A comparison of both images in Fig. 13. shows that the width of the grating lines captured using the SIBM system is more at the center compared to its sides due to swirling (marked with yellow line). This is one of the key limitations of the SIBM system. For the same above-mentioned reasons, SR-SIM using frequency shifts are difficult to implement. Figure 13(c) shows the distorted frequency components). In this study, we have restricted to implementing the optical sectioning algorithm. Additional optics or image processing must be implemented to overcome this hurdle to perform SR-SIM, which will be attempted in our future studies.

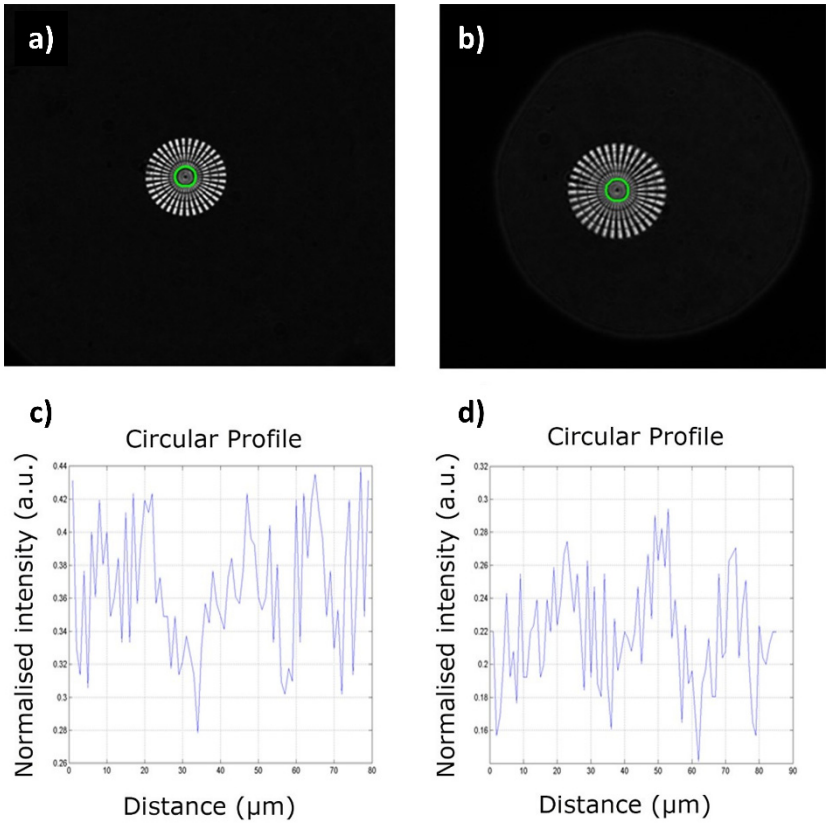

Fig. 13. Illustration of image swirling by axicon (a) Image of a grating line used for SIM using a basic microscope configuration and (b) using the SIBM configuration. (c) and (d) shows the Fast Fourier Transforms of the images (a) and (b), respectively.

References

1. M. G. L. Gustafsson, "Nonlinear structured-illumination microscopy: wide-field fluorescence imaging with theoretically unlimited resolution," Proc. Natl. Acad. Sci. U.S.A. **102**(37), 13081–13086 (2005).
2. E. Betzig, G. H. Patterson, R. Sougrat, O. W. Lindwasser, S. Olenych, J. S. Bonifacino, M. W. Davidson, J. Lippincott-Schwarts and, H. F. Hess, "Imaging Intracellular Fluorescent Proteins at Nanometer Resolution," Science **313**, 642–1645 (2006).

Optics EXPRESS

3. S. W. Hell and J. Wichmann, "Breaking the diffraction resolution limit by stimulated emission: stimulated-emission-depletion fluorescence microscopy," Opt. Lett. **19**(11), 780–782 (1994).
4. M. G. L. Gustafsson, "Surpassing the lateral resolution limit by a factor of two using structured illumination microscopy," J. Microsc. **198**(2), 82–87 (2000).
5. E. Hanssen, P. Carlton, S. Deed, N. Klonis, J. Sedat, J. DeRisi, and L. Tilley, "Whole cell imaging reveals novel modular features of the exomembrane system of the malaria parasite, Plasmodium falciparum," Int. J. Parasitol. **40**(1), 123–134 (2010).
6. S.W. Hell, Far-field optical nanoscopy. science **316**, 1153–1158 (2007).
7. M. J. Rust, M. Bates, and X. Zhuang, "Sub-diffraction-limit imaging by stochastic optical reconstruction microscopy (STORM)," Nat. Methods **3**(10), 793–796 (2006).
8. H. Shroff, C. G. Galbraith, J. A. Galbraith, and E. Betzig, "Live-cell photoactivated localization microscopy of nanoscale adhesion dynamics," Nat. Methods **5**(5), 417–423 (2008).
9. K. M. Douglass, C. Sieben, A. Archetti, A. Lambert, and S. Manley, "Super-resolution imaging of multiple cells by optimised flat-field epi-illumination," Nat. Photonics **10**(11), 705–708 (2016).
10. M. A. Schwentker, H. Bock, M. Hofmann, S. Jakobs, J. Bewersdorf, C. Eggeling, and S. W. Hell, "Wide-field subdiffraction RESOLFT microscopy using fluorescent protein photoswitching," Microsc. Res. Tech. **70**(3), 269–280 (2007).
11. N. Fang, H. Lee, C. Sun, and X. Zhang, "Sub-diffraction-limited optical imaging with a silver superlens," Science **308**(5721), 534–537 (2005).
12. N. Fang and X. Zhang, "Imaging properties of a metamaterial superlens," Appl. Phys. Lett. **82**(2), 161–163 (2003).
13. V. M. Shalaev, "Optical negative-index metamaterials," Nat. Photonics **1**(1), 41–48 (2007).
14. Z. Jacob, L. V. Alekseyev, and E. Narimanov, "Optical Hyperlens: Far-field imaging beyond the diffraction limit," Opt. Express **14**(18), 8247–8256 (2006).
15. C. Snoeyink, "Imaging performance of Bessel beam microscopy," Opt. Lett. **38**(14), 2550–2553 (2013).
16. C. Snoeyink and S. Wereley, "Single-image far-field subdiffraction limit imaging with axicon," Opt. Lett. **38**(5), 625–627 (2013).
17. S. M. Perinchery, A. Shinde, C. Y. Fu, X. J. Jeesmond Hong, M. Baskaran, T. Aung, and V. M. Murukeshan, "High resolution iridocorneal angle imaging system by axicon lens assisted gonioscopy," Sci. Rep. **6**(1), 30844 (2016).
18. R. Heintzmann and S. I. Methods, Handbook of Biological Confocal Microscopy, Springer, Boston, 265–279 (2006).
19. R. Horstmeyer, R. Heintzmann, G. Popescu, L. Waller, and C. Yang, "Standardizing the resolution claims for coherent microscopy," Nat. Photonics **10**(2), 68–71 (2016).
20. S. M. Perinchery, A. Shinde, and M. V. Matham, "Imaging behind opaque obstacle: a potential method for guided in vitro needle placement," Biomed. Opt. Express **7**(12), 5308–5324 (2016).